An analytical model and parametric analysis of ultrasound-excited infrared thermography

by Xingwang Guo*

* School of Mechanical Engineering and Automation, Beihang University, Beijing 100191, P. R. China, xingwangguo@buaa.edu.cn

Abatract

Ultrasound-excited vibrothermography (VT) is a newly developed version of IR thermographic NDT, but the relation between the defect signal and mechanical parameters is fuzzy due to the complexity of thermo-mechanical coupling and the interaction effects of multiple factors, so the design of operation conditions of VT mainly depends upon experiences up to now. In order to reveal the relations of the defect signal versus the mechanical parameters, and to enable the optimization of operation conditions, a mathematical model was presented to simulate the heat generation and heat transfer that occur during VT. The heat power produced in a crack and the temperature increase at the crack area were solved by an analytical approach. The function of the temperature increase at the crack area versus the mechanics parameters including the damp, mass, stiffness, amplitude and frequency of the stimulation force, friction coefficient and normal force in crack faces, excitation duration, etc., was deduced. The influences of mechanical parameters on the temperature increase were theoretically analyzed. The crack signature on an aluminum sample was imaged by an IR camera and compared with the theoretical predictions. The influences of experimental factors including the support condition, excitation frequency, duration and power, etc., on the crack signature were partially compared. The results show that the theoretical predictions are in agreement with the observed responses, and the influences of various mechanics parameters on VT can be quantitatively described by the analytical model presented.

1. Introduction

Ultrasound-excited vibrothermography (VT), thanks to its large-area imaging capability, selective sensitivity to particular types of defects, high test productivity, and good adaptability to irregular geometrics of structures, is a powerful tool for the inspection of defects in structures, and it is viewed as a newly developed version of IR thermographic NDT. Research in this area has been intensively carried out by several teams around the world [1-6]. The results of this research show that VT can be successfully used in the detection of cracks in metals and ceramics, as well as delaminations, disbonds and impact flaws in composite materials [7-10]. In recent years, VT has been implemented in a number of applications, particularly, in the aerospace applications [1, 4]. VT makes the capability of IR thermographic NDT extend to the detection of tightly closed and micro cracks.

The physical mechanism that gives rise to heating at crack sites is still a topic of active discussion [11-14]. It is generally agreed that local friction between contacting crack faces and mechanical hysteresis at crack tips turn a dynamically stressed crack into a heat source. The essential problem of VT is the thermo-mechanical coupling phenomenon which is complex and affected by many factors [15-16] including material, structure, support condition (i.e. boundary condition), vibration modes, excitation location [1], direction, amplitude, frequency, duration, ultrasound coupling, and holding pressure. A number of previous papers have been devoted to the numerical analysis of the heat generation by finite element method (FEM) [17-19]. Up to now, the analytical relations between the temperature rise and test conditions described by mechanics parameters have not been established.

In order to reveal the relations between temperature increase and test conditions, a theoretical model of VT was presented in this paper. The heat power produced in a crack and the temperature increase at the crack area were solved by analytical approach. The functions of the heat power and temperature increase versus the mechanics parameters were deduced. To verify the theoretical results, a VT experiment was carried out with an aluminum sample. The temperature signature at a crack region was recorded by an IR camera and compared with the theoretical predictions. The influences of test conditions on the crack signature were discussed based on the analysis and observation data.

2. Parametric analysis of vibrothermography

2.1. Vibration modeling and analysis

The modeling and analysis of VT were implemented based on the theory of forced vibration and

transient thermal conduction.

An elastic body with a crack can be imaginably divided into two parts along the crack. Let a harmonic force act on one part while another part is fixed, then the mechanical system is reduced to a single-degree-of-freedom (SDOF) model as shown in Figure 1. The dynamic behavior of the system is described by the following differential equation:
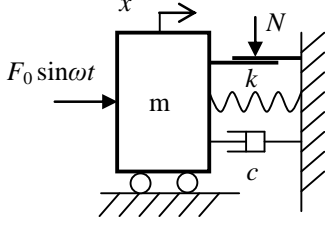
Fig.1. *Simplified mechanical model of VT*
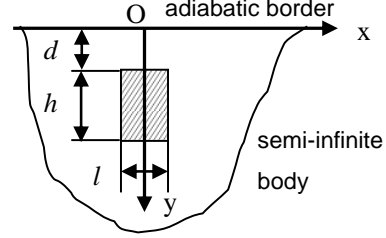
Fig. 2. *3D transient heat transfer model around a closed crack*

$$m\ddot{x} + c\dot{x} + kx = F_0 \sin \omega t - \mathrm{sgn}(\dot{x})\mu N \tag{1}$$

where m is the mass, c the damping coefficient, k the stiffness, F_0 the amplitude of the harmonic stimulation force, ω the angular frequency, μ and N are the dry friction coefficient and normal force at the crack faces respectively.

The friction and viscous damper existing in the crack dissipate the mechanical energy into heat. The viscous damper can represent anyone of heat generation mechanisms such as friction, hysteresis, plasticity and thermoelastic effect mentioned previously [13, 17, 20] by using the criteria that they dissipate the same amount of mechanical energy in one vibration circle during the stable vibration.

Eq. (1) is nonlinear due to the dry friction item. To simplify Eq. (1) to a linear equation, the dry friction should be considered as a form of equivalent viscous damping according to the rule above, and this will be described later.

At first, let us discuss the response of the system when only viscous damping exists. This results in the following ordinary differential equation:

$$m\ddot{x} + c\dot{x} + kx = F_0 \sin \omega t \tag{2}$$

The initial conditions are

$$t = 0, x = x_0, \dot{x} = \dot{x}_0 \tag{3}$$

Let's introduce the following parameters:

$$\omega_n^2 \equiv \frac{k}{m}, \quad X_0 \equiv \frac{F_0}{k}, \quad \zeta = \frac{c}{2m\omega_n} = \frac{c}{2\sqrt{mk}} = \frac{c}{c_c}, \quad \omega_d = \sqrt{1-\zeta^2}\,\omega_n, \quad \lambda = \omega / \omega_n$$

where ω_n is the undamped natural frequency (angular frequency), X_0 the displacement under a static force that equals the amplitude F_0, ζ the damping ratio, ω_d the damped natural frequency, λ the frequency ratio of the force frequency over the natural frequency, and c_c the critical damping.

In the case of small damping ($0 < \xi < 1$) and zero initial condition, the solution to Eq. (2) is the following:

$$x = Xe^{-\zeta\omega_n t}\beta\lambda[\frac{\omega_n(2\zeta^2 - 1 + \lambda^2)}{\omega_d}\sin\omega_d t + 2\zeta\cos\omega_d t] + X\sin(\omega t - \psi) \tag{4}$$

where

$$X = \frac{X_0}{\sqrt{(1-\lambda^2)^2 + (2\zeta\lambda)^2}}, \quad \psi = \arctan\frac{2\zeta\lambda}{1-\lambda^2}, \quad \beta \equiv \frac{X}{X_0} = \frac{1}{\sqrt{(1-\lambda^2)^2 + (2\zeta\lambda)^2}}$$

The heat power dissipating at the damper is

$$P(t) = c\dot{x}^2$$

$$= \frac{2\zeta F_0^2 \beta^2 \lambda^2}{\sqrt{mk}} \{ e^{-2\zeta\omega_n t} \beta^2 z^2 \frac{1}{2} [1 - \cos(2\omega_d t + 2\phi)] - 2e^{-\zeta\omega_n t} \beta z \sin(\omega_d t + \phi) \cos(\omega t - \psi) + \frac{1}{2} [1 + \cos(2\omega t - 2\psi)] \} \quad (5)$$

$$= P_1(t) + P_2(t) + P_3(t)$$

where

$$z = \sqrt{\frac{\zeta^2 (1 + \lambda^2)\omega_n^2}{\omega_d^2} + (1 - \lambda^2)^2}, \quad \tan\phi = \frac{(1 - \lambda^2)\omega_d}{\zeta(1 + \lambda^2)\omega_n}$$

The first and second item in Eq. (5) are transient components which disappear quickly, while the third item $P_3(t)$ is the stable, persistent and dominant portion of the solution, and its mean is the following:

$$\bar{P}_3 = P_c = \frac{cF_0^2 \omega_n^2}{2k^2} \beta^2 \lambda^2 \tag{6}$$

For any possible non viscous damping at cracks, such as the dry friction, it can be considered as equivalent viscous damping based on the criteria that the two damping dissipate equal amount of energy in one period during the stable vibration. The equivalent damping coefficient of the dry friction is the following:

$$c_f = \frac{4\mu N}{\pi\omega X} \tag{7}$$

The mean stable power corresponding to the friction damping is the following:

$$\bar{P}_3 = P_f = \frac{2\mu N F_0 \omega_n}{\pi k} \beta\lambda \tag{8}$$

It can be seen from Eq. (8) that the normal force has the same importance as the amplitude of the stimulation force.

When the viscous damping and try friction exist simultaneously, the damping coefficient c in Eq. (5) should be replaced by the total equivalent damping coefficient c_t as expressed in Eq. (9):

$$c_t = c + c_f \tag{9}$$

The corresponding mean persistent power is the sum of Eqs. (6) and (8):

$$\bar{P}_3 = P_c + P_f \tag{10}$$

2.2. Heat conduction modeling and analysis

The body with a crack can be considered as a semi-infinite isotropic body with an internal rectangular plane heat source corresponding to the closed part of the crack. Fig. 2 shows the 3D heat transfer model, where the size and depth of the plane source are $l \times h$ and d respectively, the total heat power $P(t)$ is uniformly distributed at the closed crack face. For the sake of simplicity, the boundary is considered to be adiabatic.

The temperature increase at the surface spot O over the closed crack is the following:

$$\theta(t) = \frac{1}{2C\rho(\pi\alpha)^{\frac{3}{2}} lh} \int_d^{d+h} \int_0^{\frac{l}{2}} \int_0^t P(\tau)(t-\tau)^{-\frac{3}{2}} e^{-\frac{R^2}{4\alpha(t-\tau)}} d\tau dx dy \tag{11}$$

where ρ is the density, C the specific heat, α the diffusivity, $R^2 = x^2 + y^2$.

It is reasonable to ignore the transient components in Eq. (5) and only count the stable persistent component, i.e. to substitute $\bar{P}_3$ (Eq.(6)) for $P(t)$. This results in:

$$\theta(t) = \theta_{sm}(t) = \frac{F_0^2}{\sqrt{mk} \cdot \pi\kappa lh} \cdot \frac{\zeta\lambda^2}{(1-\lambda^2)^2 + (2\zeta\lambda)^2} \int_d^{d+h} \int_0^{\frac{l}{2}} \frac{1}{\sqrt{x^2 + y^2}} [1 - \mathrm{erf}(\frac{\sqrt{x^2 + y^2}}{\sqrt{4\alpha t}})] dx dy \tag{12}$$

where κ is the thermal conductivity, $\kappa = C\rho\alpha$, $\mathrm{erf}(\bullet)$ is the error function:

$$\mathrm{erf}(x) = \frac{2}{\sqrt{\pi}} \int_0^x e^{-u^2} du \tag{13}$$

3. Experimental setup and sample

To verify the theoretical predictions, a VT experiment was carried out with an aluminum sample. An ultrasound-excited VT system (Fig. 3) developed at the Beihang University, China, has been used. The system includes an IR camera produced by FLIR, an ultrasonic device, a mounting frame, and a computer with specialized software for image acquisition and processing. The ultrasonic device includes an ultrasonic piezoelectric transducer and a booster driven by an ultrasound source. Two ultrasonic devices were used respectively. These devices have different specifications: (1) frequency of 20 kHz and nominal power of 1.5 kW, (2) frequency of 15 kHz and tunable nominal power up to 2.6 kW.
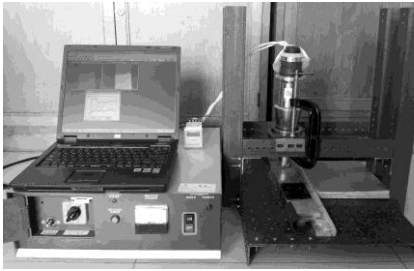
Fig. 3. Ultrasound-excited VT system (except IR camera)
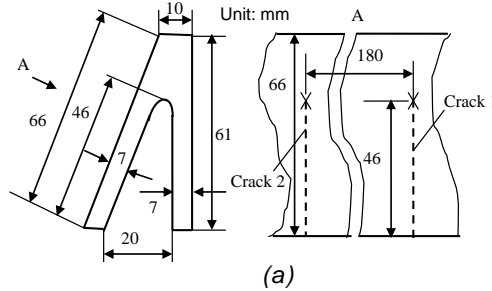
Fig. 4. V-profile aluminum alloy beam: (a) sample scheme, (b) sample photo

The sample is a 490 mm-long and 7 mm-thick V-profile beam made of aluminum alloy (Fig. 4). Two through-thickness cracks were produced on the 66 mm-wide side surface of the beam. The two cracks emanate from the thin edge to the thick edge of the beam. The first crack (cracks 1) was taken as an example to be monitored by the IR camera.

Both the ultrasonic exciter and the sample were held by the mounting frame. The booster was pressed against the sample with a screw. A 0.16 mm-thick piece of plastic was inserted between the booster and the sample to couple ultrasound propagation. To increase surface emissivity and reduce background reflections, the monitored area was coated with a water-based black paint before testing.
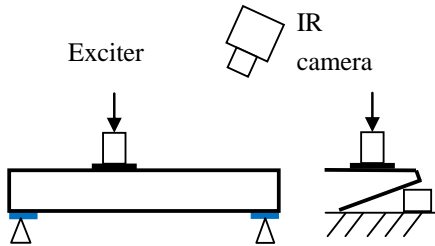
Fig. 5. Horizontal support scheme
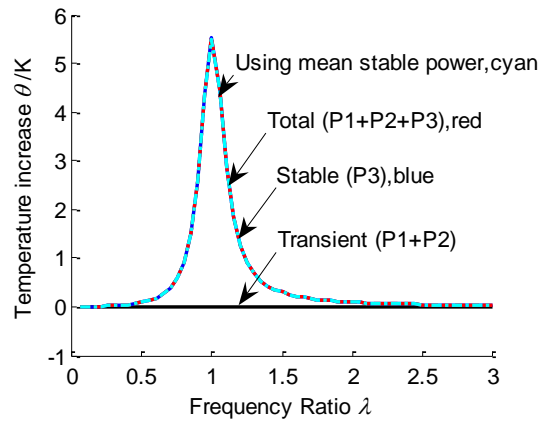
Fig. 6. Temperature increases corresponding to different components in Eq. (8), taking $F_0 = 250$ N and $\zeta = 0.1$

The whole crack comprises of an open and closed section. During vibration, the heat is generated only at the closed area where the two crack faces contact each other. The natural frequency is related with the support condition. In the horizontal support scheme as shown in Fig.5, the tested plate of the sample is fixed as a cantilever beam. Some parameters were approximately evaluated as the following: $d = 0$, $h = 0.007$ m, $l = 0.001$ m, $\kappa = 126$ W·m^{-1}K^{-1}, $m = 0.160$ kg, $f_n = 16.75$ kHz ($f_n = \omega_n/(2\pi)$).

4. Theoretical predictions

Take $F_0 = 250\,\text{N}$ and $\zeta = 0.1$ for the sample supported as in Fig. 5, the temperature increases corresponding to different components of the heat power in Eq. (5) were shown in Fig.6. It can be seen that the contribution of the transient components of the heat power to the temperature increase nears zero, and the temperature increase computed by using the mean of the stable component of the heat power (i.e. $\bar{P}_3$) is exact enough. So the vibration in VT can be completely simplified into a stable forced vibration problem.

The influences of the frequency ratio and damping ratio on the temperature increases were shown in Fig. 7. It can be seen that when resonance occurs ($\lambda \approx 1$), the temperature increase gets its maximum; the smaller the damping ratio, the greater the temperature increase.
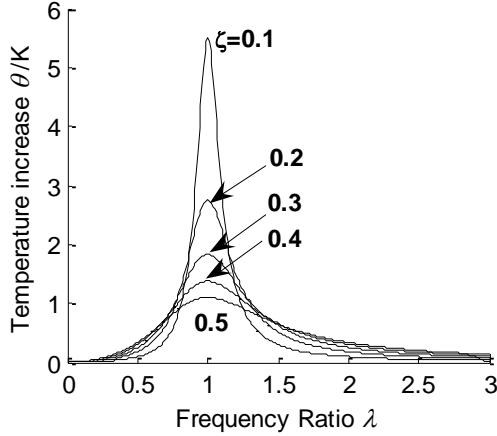
Fig. 7. *Temperature increases vs frequency ration for different damping ratios at time* $t = 0.3$ *s, taking* $F_0 = 250\,\text{N}$
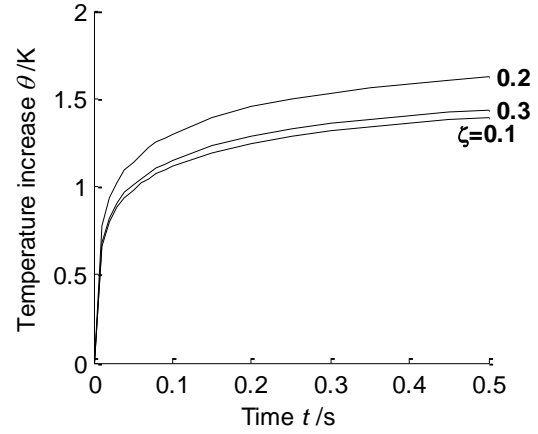
Fig. 8. *Temperature increase evolutions for different damping ratios, taking* $\lambda = 1.194$, $F_0 = 250\,\text{N}$

The temperature increase evolutions for different damping ratios were shown in Fig. 8 when taking $\lambda = 1.194$ ($f = 20\text{kHz}$) and $F_0 = 250\,\text{N}$.

5. Experimental results

In the first experiment, the V-profile beam was mounted horizontally with the monitored plate as a short cantilever (Fig. 5), and it was continuously excited near the middle with 20 kHz ultrasonic waves. The IR camera acquired IR images with a frequency of 60 Hz. The crack signature in spatial and time domain was shown in Fig. 9 and Fig. 10 respectively.
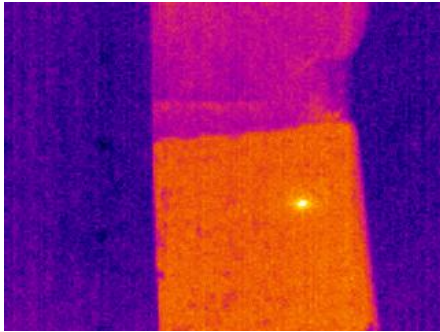
Fig. 9. *A typical* **raw** *IR image in the first experiment (t=0.25s)*
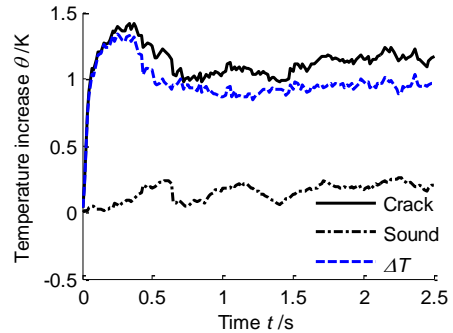
Fig. 10. *The evolution of temperature parameters in the first experiment*

The operation conditions were varied to observe the corresponding changes of the crack signature, and the experimental results were summarized in table 1.

Table 1. *Operation conditions and experimental results for the aluminum alloy sample*

No.	Support and excitation	f /kHz	P_0 /kW	F_h /N	Duration /s	θ_m /K	$t_m(\theta)$ /s	ΔT_m /K	$t_m(\Delta T)$ /s
1	As shown in Fig. 5	20	1500	~50	Continuous	1.42	0.350	1.33	0.267
2	As shown in Fig. 5	20	1500	~50	2.7	1.32	0.433	1.24	0.333
3	As shown in Fig. 11	20	1500	~50	Continuous	~0	N/A	N/A	N/A
4	As shown in Fig. 5	15	433	~50	3.2	0.80	0.433	0.73	0.333

Note: f -the excitation frequency, P_0 -the nominal power used, F_h -the holding (static contact) pressure, θ_m -the maximum temperature increase, $t_m(\theta)$ -the time when θ_m occurs, ΔT_m -the maximum temperature difference between crack and sound area, $t_m(\Delta T)$ -the time when ΔT_m occurs

The temperature increase evolutions obtained by the theory (Eq. (12)) and experiment were compared in Fig. 12. A damping ratio of 0.1 was supposed by trials due to the lack of knowledge about the frictional and damped characteristics of the crack. It is can be seen from Fig. 12 that the theoretical predictions were in good agreement with the observed responses at early time. The earlier drops of the experimental curves during stimulation were attributed to the fixture's loosing after a suddenly stimulation.
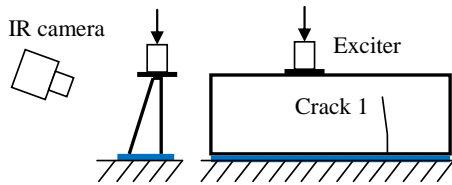
Fig. 11. *Vertical support scheme*
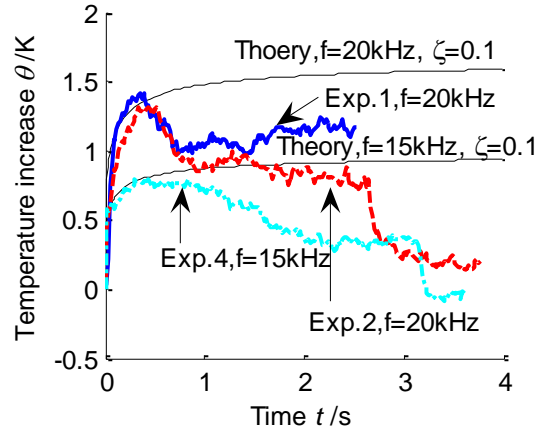
Fig. 12. *Temperature increase evolutions obtained by the theory (Eq. (12)) and experiment*

6. Conclusions

(1) The analytical model presented reflects the major aspects of VT. The theoretical predictions are in good agreement with the observed responses, and the influences of various mechanics parameters on VT can be quantitatively described by the analytical model.

(2) The basic relation of the temperature increase versus the mechanics parameters can be expressed with Eq. (12). It explicitly describes all of the influences of various mechanics parameters on the temperature rise and indicates that: the temperature increase is proportional to the square of the stimulation force amplitude; the temperature increase is a non-linear function of the frequency ratio and damping ratio; the cracks in heavy and rigid structures are more difficult to detect due to the greater mass and stiffness.

(3) The crack signature can be greatly enhanced when the sample is stimulated near its resonant region.

(4) The contribution of the transient heat-power components, which correspond to the transient vibration components, to the temperature increase nears zero. The temperature increase is almost completely determined by the stable permanent vibration. Based on this conclusion, the vibration analysis can be greatly simplified by only considering the stable vibration.

(5) In the crack detection of aluminum, short-pulse (burst) stimulation (from 0.4 to 1 s) is sufficient, while in the case of non-metals, the necessary excitation duration may be relatively long.

Although the modeling accuracy of the SDOF model is poor comparing with the FEM, the dominant relations between the heat power and mechanics parameters can be established in the form of analytic function. To improve the modeling accuracy, the modeling of VT by using multiple-degree-of-freedom forced vibration model should be researched in future.

REFERENCES

[1] Han X., Zhao S., Zhang D., "Develop sonic infrared imaging NDE for quantitative assessment on damage in aircraft composite structures". Proceedings of 11th Quantitative InfraRed Thermography conference, paper QIRT2012-185, 11-14 June, Naples Italy, 2012
[2] Dillenz A., Zweschper T., Busse G., "Burst phase angle thermography with elastic waves". In: Maldague X. P., Rozlosnik A. E., Proc SPIE, Vol.4710, Thermosense XXIV, Bellingham: SPIE, pp.572-577, 2002.

[3] Piau J. M. A., Bendada A., Maldague X. P. V., "Ultrasound vibrothermography applications for nondestructive discontinuity detection". Materials Evaluation, Vol.66(10), pp.1047-1052, 2008.

[4] Ibarra-Castanedo C., Piau J. M., Guilbert S., Avdelidis N. P., Genest M., Bendada A., Maldague X. P. V.. "Comparative study of active thermography techniques for the nondestructive evaluation of honeycomb structures". Research in Nondestructive Evaluation, Vol.20(1), pp.1-31, 2009.

[5] Holland S. D., Uhl C., Ouyang Z., et al, "Quantifying the vibrothermographic effect". NDT&E International, Vol.44, pp.775–782, 2011.

[6] Vavilov, V. P.; Nesteruk, D. A., "Comparative analysis of optical and ultrasonic stimulation of flaws in composite materials". Russian Journal of Nondestructive Testing, Vol. 46(2), pp.147-150, 2010.

[7] Favro L. D., Han X., Ouyang Z., et al, "Progress in thermosonic crack detection". In: Rozlosnik A. E., Dinwiddie R. B., Proc SPIE, Thermosense XXIII, Bellingham: SPIE, pp.546-549, 2001.

[8] Bussel G., Dillenz A., Zweschper T., "Defect-selective imaging of aerospace structures with elastic-wave-activated thermography". In: Rozlosnik A. E., Dinwiddie R. B., Proc SPIE, Thermosense XXIII, Bellingham: SPIE, pp.580-586, 2001.

[9] Favro L. D., Han X., Ouyang Z., et al, "Thermosonic imaging of cracks and delaminations". Progress in Natural Science, Vol.11(Suppl), pp.133-136, 2001.

[10] Burke M. W., Miller W. O., "Status of VibroIR at Lawrence Livermore National Laboratory". In: Burleigh D. D., Cramer K. E., Peacock G. R., Proc SPIE, Thermosense XXVI, Bellingham: SPIE, pp.313-321, 2004.

[11] Montanini R., Freni F., "Investigation of heat generation sources in sonic infrared thermography using laser Doppler vibrometry". Proceedings of 11th Quantitative InfraRed Thermography conference, paper QIRT2012-177, Naples, Italy, 11–14 June, 2012.

[12] Han X., Islam M. S., "Progress on developing acoustic-infrared imaging NDE: studying motions in crack faces". Proc. SPIE, Vol.7647, 76473L-1-6, 2010.

[13] Renshaw J., Chen J. C., Holland S. D., "Thompson RB. The.sources.of heat generation in vibrothermography". NDT&E International, Vol.44, pp.736-739, 2011.

[14] Homma C., Rothenfusser M., Baumann J., Shannon R., "Study of the heat generation mechanism in acoustic thermography". AIP Conf. Proc. 820, 566; doi: 10.1063/1.2184578, 2006.

[15] S M Shepard, Experimental considerations in vibrothermography, In: D D Burleigh, K E Cramer, G R Peacock. Proc SPIE Thermosense XXVI. Bellingham: SPIE, 2004, 332-335

[16] Mayton D., Spencer F., Alvarez C., "Characterizing the effects of sonic IR variables on turbine disk inspection using a design of experiments approach". In: Thompson D. O., Chimenti D. E., Review of progress in quantitative nondestructive evaluation, Vol.24, Golden, Colorado (USA): AIP, pp.642-649, 2005.

[17] Rizi A. S., Hedayatrasa S., Maldague X., Vukhanh T., "FEM modeling of ultrasonic vibrothermography of a damaged plate and qualitative study of heating mechanisms". Infrared Physics & Technology, Vol. 61, pp.101-110, 2013.

[18] Han X., Islam M. S., Newaz G., Favro L. D., Thomas R. L., "Finite element modeling of the heating of cracks during sonic infrared imaging". Journal of Applied Physics, Vol.99, 074905; doi: 10.1063/1.2189023, 2006.

[19] Pieczonka L. J., Staszewski W. J., Aymerich F., Uhl T., Szwedo M., "Numerical simulations for impact damage detection in composites using vibrothermography". Materials Science and Engineering, Vol.10, 012062; doi:10.1088/1757-899X/10/1/012062, 2010.

[20] Rantala J., Wu D., Busse G., "Amplitude-modulated lock-In vibrothermography for NDE of polymers and composites". Res Nondestr Eval, Vol.7, pp.215-228, 1996.